ELSEVIER

Chemical Geology 174 (2001) 349–363

CHEMICAL GEOLOGY
INCLUDING
ISOTOPE GEOSCIENCE

www.elsevier.com/locate/chemgeo

Cationic environment in silicate glasses studied by neutron diffraction with isotopic substitution

L. Cormier [a,*], G. Calas [a], P.H. Gaskell [b]

[a] *Laboratoire de Minéralogie-Cristallographie, Universités Paris 6 et 7 et Insitut de Physique du Globe de Paris et UMR CNRS 7590, 4 place Jussieu, Paris Cedex 05 75252, France*

[b] *Cavendish Laboratory, University of Cambridge, Madingley Road, Cambridge CB3 0HE, England, UK*

Accepted 9 February 2000

Abstract

The method of neutron diffraction coupled with isotopic substitution is presented and recent investigations on the environment around cations in silicate (Ti in $K_2O \cdot TiO_2 \cdot 2SiO_2$, Ca and Ni in $2CaO \cdot NiO \cdot 3SiO_2$) and aluminosilicate (Li in $Li_2O \cdot Al_2O_3 \cdot 2SiO_2$) glasses are reviewed. The examination of the cation-centered pairs obtained from the first difference function presents striking similarities for all investigated cations. These functions indicate a well-defined short- and medium-range environment around cations. The local site generally presents a lower coordination number than that found in the crystals of similar composition. The environment around Ti in vitreous $K_2O \cdot TiO_2 \cdot 2SiO_2$ corresponds to a square-based pyramid and direct TiO_5–TiO_5 linkages were observed experimentally in the second difference function, contrary to crystals. A detailed description of the cation site distortion for Li and Ca may be given by this method. The distribution of cations at medium range, which can be extracted by the double difference method, reveals the presence of cation-rich regions in silicate glasses. The cation–cation distances often indicate a two-dimensional character in the cationic organization. On the contrary, Li-aluminosilicate glass shows a more homogeneous cation distribution, in relation with the charge-compensating role of Li in this glass. This non-homogeneous distribution of cations may be related to the nano-inhomogeneities proposed in the models of supercooled liquids.

Keywords: Glasses; Structure; Medium-range order; Neutron diffraction; Isotopic substitution

1. Introduction

Knowing the extent of the structural order in silicate glasses and melts is an important goal to better understand their properties. However, due to the non-directional character of cation–oxygen bonds, disorder effects strongly limit the accessible information concerning the medium-range order around cations. Neutron diffraction has been widely used to investigate the structure of silicate glasses and melts (Gaskell, 1991; Waseda and Suito, 1977), since diffraction methods give access to both short- and medium-range order (up to ≈ 15 Å). For multi-component systems, the overlapping of the coordination shells limits the structural information which can be extracted from the data. The use of chemically selective techniques such as X-ray absorption

* Corresponding author. Tel.: +33-1-4427-5065; fax: +33-1-4427-5064.

E-mail address: cormier@lmcp.jussieu.fr (L. Cormier).

0009-2541/01/$ - see front matter
PII: S0009-2541(00)00325-9

spectroscopy (XAS) or anomalous wide angle X-ray scattering (AWAXS) has proved useful for studying the environment around cations in silicate glasses (Waseda, 1984; Cormier et al., 1996). These techniques are suitable for relatively heavy elements and, in the case of XAS, for dilute content. However, disorder effects limit a quantitative evaluation beyond the first or second coordination shell in XAS spectra, and AWAXS data suffer from the problem of limited resolution and statistics.

Alternatively, neutron diffraction combined with isotopic substitution can be used to separate the partial pair distribution functions associated with one specific element in the sample. The geometry of the coordination shell, the intercationic distances, the number of cations involved in the medium-range organization and their relationships with the silicate framework can all be determined by this technique. The first part of this paper presents the main concepts of neutron diffraction, with an emphasis on the isotopic substitution method. In the second part, the study of a potassium titanosilicate glass ($K_2O \cdot TiO_2 \cdot 2SiO_2$) is used to illustrate the usefulness of this method for providing very selective information about structural cationic organization. Finally, we present evidence showing the strong similarity between the structural organization of different cations in silicate glasses (Ti in $K_2O \cdot TiO_2 \cdot 2SiO_2$, Li in $Li_2O \cdot Al_2O_3 \cdot 2SiO_2$ and Ca and Ni in $2CaO \cdot NiO \cdot 3SiO_2$), indicating a heterogeneous structure of silicate glasses.

2. Theoretical outline

Neutron diffraction by amorphous solids or liquids shows important differences with X-ray diffraction (see, e.g., Wright, 1974). As X-rays are scattered by electrons, uncharged neutrons directly interact with nuclei. As a consequence, they can be used to determine the structural position of light Z elements, such as H or Li. For instance, the influence of water on the medium-range structure of glasses has been investigated on hydrous sodium tetrasilicate glasses (Zotov et al., 1996). Due to the small size of atomic nuclei as compared to neutron wavelength, scattering is independent of the diffraction angle. This is particularly advantageous as the interaction with a given atom does not vary simply with Z, as in the case of X-rays, but may be very different for two neighbor elements and even for isotopes of the same element. This last property is at the basis of the isotopic substitution method which is explained below.

2.1. Neutron diffraction

In a conventional total diffraction experiment, neutrons are scattered elastically and inelastically (as a result from the interaction of the neutron beam with thermal vibrations). Only elastic scattering gives information on the static radial structure of the glass and is given by the structure factor $S(Q)$, in which Q is the amplitude of the scattering vector, defined by $Q = 4\pi \sin\theta/\lambda$ (2θ is the scattering angle and λ the wavelength of the neutrons). A correlation function $G(r)$ is used to describe the radial interatomic distances in the real space, defined as the probability of finding an atom at position r.

For isotropic materials, the static structure factor may be written as:

$$S(Q) = 1 + 4\pi\rho_0 \int_0^\infty r^2 \left[g(r) - 1 \right] \frac{\sin(Qr)}{Qr} \mathrm{d}r, \tag{1}$$

in which r is the interatomic distance, and $g(r)$ is the pair correlation function. $g(r)$ describes the local density fluctuations around unity.

For polyatomic materials, the structure factor and the correlation function are a weighted sum of all the partial structure factors, $S_{\alpha\beta}(Q)$, and of all the partial pair correlation functions (PPCFs), $g_{\alpha\beta}(r)$, respectively (Faber and Ziman, 1964),

$$S(Q) = \sum_{\alpha\beta} W_{\alpha\beta} S_{\alpha\beta}(Q), \tag{2}$$

$$G(r) = 4\pi r \rho_0 \sum_{\alpha\beta} W_{\alpha\beta} \left[g_{\alpha\beta}(r) - 1 \right], \tag{3}$$

in which $W_{\alpha\beta}$ is the weighting factor, $W_{\alpha\beta} = c_\alpha c_\beta b_\alpha b_\beta$, and c_i and b_i are the atomic concentration and the neutron scattering length of atoms of type i, respectively.

In practice, various functions may be used to describe the structure of a scattering material: the reduced pair correlation function $G(r)$, the total correlation function, $T(r) = 4\pi r\rho_0 \sum_{\alpha\beta} W_{\alpha\beta} g_{\alpha\beta}(r)$, and the radial distribution function, $\mathrm{RDF}(r) = 4\pi r^2 \rho_0 \sum_{\alpha\beta} W_{\alpha\beta} g_{\alpha\beta}(r)$ are used alternatively.

For neutrons, the scattering lengths, b, are independent of Q, whereas the X-ray atomic scattering factors vanish to zero at high Q-values. Not only does this property aid data reduction, but a large Q-range is accessible by neutron diffraction (0.2–50 Å^{-1} with pulsed sources), thus permitting direct determination of both local- and medium-range order with great accuracy. Though XAS can be employed for trace concentration levels and can detect minor amounts of coordination sites (see, e.g., Brown et al., 1995), coordination numbers and interatomic distances are less accurately evaluated than in neutron diffraction measurements, since the low Q-values cannot be used in the classical EXAFS formulation (Brown et al., 1995). Hard X-rays (Poulsen et al., 1995) offer access to a Q-range (0.8–32 Å^{-1}) comparable to neutrons but the noise/signal ratio in neutron diffraction is lower and the data corrections are better understood by theory than in X-ray diffraction. Absolute normalization using a vanadium standard is also possible in neutron diffraction. However, for materials with large inelasticity or absorption corrections (such as Li and H), caution is required in neutron data analysis.

2.2. Isotopic substitution

The $G(r)$ function is dominated by the heavily weighted PPCFs which are usually, in silicates, the Si–O, O–O and Si–Si pairs. Above about 3 Å, these contributions are buried among the correlations with smaller weighting factors (e.g., the PPCFs associated with modifiers). Structural models can be used to interpret $G(r)$ functions, but the structural models fitting the data are not unique. Ideally, it would be suitable to obtain each PPCF to describe the complete structure. For a material containing n elements, this requires $n(n+1)/2$ independent experiments, which becomes impractical for multicomponent systems. However, some partials can be isolated in neutron diffraction experiments by modifying the neutron scattering length, b, which can vary sharply for different elements or for different isotopes of the same element. The first property is used for isomorphic substitution (exchange of elements playing identical role in the structure) while the second leads to a more rigorous contrast technique — the isotopic substitution.

The isotopic substitution technique consists of measuring the diffraction for specimens, which have the same thermal history and are identical apart from the isotopic composition of one component, M. In two separate experiments, two total structure factors are obtained which differ by the weights of the partials involving M due to the variation of b_M:

$$S(Q) = \sum_{\substack{\alpha\beta \\ \alpha,\beta\neq M}} c_\alpha c_\beta b_\alpha b_\beta \left(S_{\alpha\beta}(Q) - 1\right) + \sum_{\substack{\alpha M \\ \alpha\neq M}} c_\alpha c_M b_\alpha b_M \left(S_{\alpha M}(Q) - 1\right) + c_M^2 b_M^2 \left(S_{MM}(Q) - 1\right), \quad (4)$$

$$S'(Q) = \sum_{\substack{\alpha\beta \\ \alpha,\beta\neq M}} c_\alpha c_\beta b_\alpha b_\beta \left(S_{\alpha\beta}(Q) - 1\right) + \sum_{\substack{\alpha M \\ \alpha\neq M}} c_\alpha c_M b_\alpha b'_M \left(S_{\alpha M}(Q) - 1\right) + c_M^2 b_M'^2 \left(S_{MM}(Q) - 1\right). \quad (5)$$

By subtracting the two equations above, the first term in the right-hand side is canceled and a first difference function, $\Delta_{M-\alpha}(Q)$, is obtained. By Fourier transforming this differential structure factor, one obtains a correlation function, $G_{M-\alpha}(r)$, which is the sum of all the PPCFs involving M:

$$G_{M-\alpha}(r) = \frac{2}{\pi}\int_0^{Q_{\max}} \Delta_{M-\alpha}(Q) Q \sin(Qr)\,\mathrm{d}Q = 2\sum_{\alpha\neq M} c_\alpha c_M b_\alpha \left(b_M - b'_M\right) g_{M\alpha}(r) + c_M^2\left(b_M^2 - b_M'^2\right) g_{MM}(r). \quad (6)$$

This function is similar to the difference calculated in AWAXS measurements (see, e.g., Cormier

et al., 1996) or the Fourier transform of the EXAFS signal. However, a wider Q-range and better statistics can be realized with neutrons resulting in a more accurate determination of the coordination numbers, better resolution and extended range of accurate data in r-space.

By measuring the neutron diffraction intensities for three isotopically substituted samples, two first difference functions can be calculated:

$$\Delta_{M-\alpha}(Q) = 2\sum_{\alpha\neq M} c_\alpha c_M b_\alpha (b_M - b'_M)(S_{M\alpha}(r) - 1) + c_M^2\left(b_M^2 - b_M'^2\right)(S_{MM}(Q) - 1), \quad (7)$$

$$\Delta'_{M-\alpha}(Q) = 2\sum_{\alpha\neq M} c_\alpha c_M b_\alpha (b'_M - b''_M)(S_{M\alpha}(r) - 1) + c_M^2\left(b_M'^2 - b_M''^2\right)(S_{MM}(Q) - 1). \quad (8)$$

If the condition $b_M - b'_M = b'_M - b''_M$ is fulfilled, the $\Delta_{M-\alpha}(Q)$ and $\Delta'_{M-\alpha}(Q)$ functions differ only by the second term on the right-hand side that involves M–M correlations. Subtracting these two first difference datasets eliminates all the terms except that associated with M–M pairs and hence, a second difference signal, $\Delta(\Delta_{M-\alpha}(Q))$, is obtained:

$$\Delta(\Delta_{M-\alpha}(Q)) = \frac{1}{2}c_M^2(b_M - b''_M)^2(S_{MM}(Q) - 1). \quad (9)$$

In real space, the M–M pair correlation function, G_{MM}, describes, directly, the distribution of M in the structure:

$$G_{MM}(r) = \frac{2}{\pi}\int_0^{Q_{max}}\Delta(\Delta_{M-\alpha}(Q))Q\sin(Qr)\mathrm{d}Q = c_M^2\frac{(b_M - b''_M)^2}{2}g_{MM}(r). \quad (10)$$

Only the double difference allows, experimentally, the extraction of one partial structure factor. Ideally, the $\Delta(\Delta_{M-\alpha}(Q))$ function is proportional only to the partial structure factor $S_{MM}(Q)$ (see Eq. (9)). By using the experimental values of $K_2O \cdot TiO_2 \cdot 2SiO_2$ glass (Cormier et al., 1998a), we obtain $\Delta(\Delta_{Ti-\alpha}(Q)) \approx 0.26[S_{TiTi}(Q) - 1]$. This is a very weak signal (typically less than 1% of the total signal) which contains a considerable level of random noise and is extremely sensitive to systematic errors associated with composition, variations between the samples, errors in b values, etc. However, systematic errors can be minimized by an accurate determination of the chemical and isotopic composition.

In isotopic substitution, the difference in the neutron scattering lengths of the different isotopes has to be large ($b - b' > 3$ fm) in order to obtain a good difference signal. In addition, the need of concentrations, usually higher than 5 at.%, does not allow the investigation of dilute elements. Isotopes must be stable, non-highly absorbing and have a known scattering length. These criteria limit the number of elements suitable for the isotopic substitution technique. Several cations in silicate glasses have been studied by this method recently, taking advantage of the development of new generation neutron sources (Gaskell, 1993; Gaskell et al., 1991).

3. Results and discussion

3.1. Experimental

Glasses of composition $K_2O \cdot TiO_2 \cdot 2SiO_2$, $Li_2O \cdot Al_2O_3 \cdot 2SiO_2$ and $2CaO \cdot NiO \cdot 3SiO_2$ were prepared using appropriate quantities of oxides and carbonates by quenching from the melt (details of the synthesis can be found in Cormier, 1996). The following isotopes of Ti, Li, Ca and Ni were used: $^{46-}$, $^{48-}$ and ^{mix}Ti (i.e., an equal mixture of $^{46-}$ and ^{48}Ti isotopes), $^{6-}$ and ^{7}Li, $^{44-}$, ^{nat} and ^{mix}Ca (in which ^{nat}Ca refers to the natural isotopic composition and ^{mix}Ca to an equal mixture of $^{nat-}$ and ^{44}Ca isotope) and $^{62-}$, ^{nat} and ^{mix}Ni (^{mix}Ni refers to an equal mixture of $^{nat-}$ and ^{62}Ni isotope). Neutron total diffraction experiments were carried out on the SANDALS diffractometer at the ISIS pulsed neutron source (Rutherford Laboratory, UK) and on the 7C2

diffractometer on the ORPHEE reactor (Laboratoire Léon Brillouin, Saclay, France). Diffracted intensities were recorded at room temperature for the specimens in the container, the empty container and a vanadium rod used for absolute normalization. The data analysis follows the standard procedures for absorption, inelasticity and multiple scattering corrections (Hannon et al., 1990; Soper et al., 1989). The advantage of the ISIS source is to give access to a wider range of scattering vectors ($0.2\ \text{Å}^{-1} < Q < 50\ \text{Å}^{-1}$) compared to steady state reactors ($0.3\ \text{Å}^{-1} < Q < 16\ \text{Å}^{-1}$) and thus, a better resolution of the data in real space. We will present the various steps of the analysis in the case of the Ti-silicate glass. In the second part, we will discuss the general structural behavior of cations in silicate and aluminosilicate glasses, the definition of their coordination shells, and the structural order involving cations over several interatomic distances.

3.2. Structural study of a potassium titanosilicate glass

The total correlation functions, $G(r)$, for the $K_2O \cdot TiO_2 \cdot 2SiO_2$ glass are shown in Fig. 1 for the three investigated samples that contain almost pure ^{48}Ti, ^{46}Ti and an equal mixture of ^{48}Ti and ^{46}Ti isotopes. The Si–O correlations are responsible for an intense and narrow peak at 1.62 Å. A strong peak at 2.68 Å corresponds to O–O pairs (from the Si and Ti polyhedra) as well as K–O pairs. The intensity of the peak near 2 Å changes according to the negative or positive sign of b for the ^{48}Ti or ^{46}Ti isotope (Fig. 1, inset). As in crystalline references, the feature at 2 Å

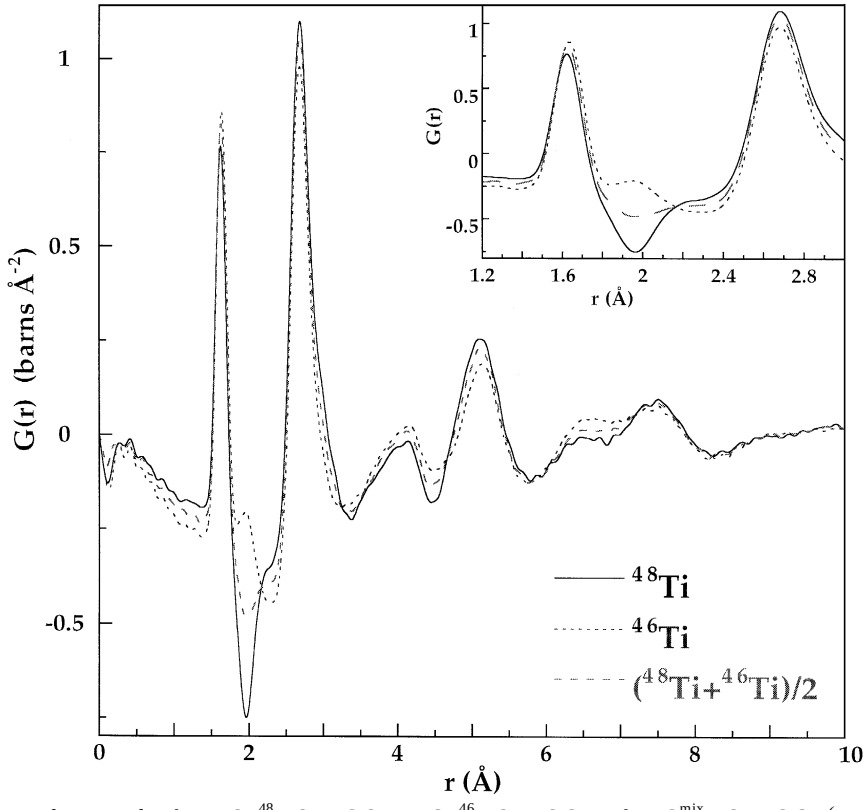

Fig. 1. Total correlation functions for the $K_2O \cdot {}^{48}TiO_2 \cdot 2SiO_2$, $K_2O \cdot {}^{46}TiO_2 \cdot 2SiO_2$ and $K_2O^{mix}TiO_2 \cdot 2SiO_2$ (mix = [^{48}Ti + ^{46}Ti]/2). The inset shows the region of the first Ti–O coordination shell where the variations in intensities are due to the positive and negative sign of the neutron scattering lengths for ^{46}Ti and ^{48}Ti isotopes.

can be ascribed to Ti–O correlations. The usefulness of the first difference function, $G_{\mathrm{Ti}-\alpha}(r)$, is to cancel the heavily weighted Si–O and O–O correlations (Fig. 2). It then appears that the first shell of oxygen neighbors around Ti can be deconvoluted into two distinct Ti–O distances at 1.68 and 1.96 Å. The Ti site corresponds to a square base pyramid with four O at 1.96 Å and one O (also referred to as titanyl oxygen) at 1.68 Å (Fig. 2, inset). These results are in agreement with previous neutron diffraction (Yarker et al., 1986) and EXAFS studies (Farges et al., 1996). By contrast to EXAFS, isotopic substitution neutron diffraction method is able to resolve the two Ti–O distances due to the larger *Q*-space available, which gives narrower Fourier transform components. A small peak near 2.6 Å is observed in the $G_{\mathrm{Ti}-\alpha}(r)$ function and may come from an incomplete subtraction of the O–O and/or the K–O pairs. It should be noted that the same small peak is also present in the $G_{\mathrm{Ti}-\alpha}(r)$ function of Yarker et al. (1986). A second broad feature between 3 and 4.7 Å can be seen in the $G_{\mathrm{Ti}-\alpha}(r)$ function with four peaks that can be assigned to Ti–Si, Ti–K, Ti–Ti and second Ti–O(2) distances, according to comparisons with crystalline titanosilicates and titanates. However, no direct assignment can be made to specific atomic contributions using first difference functions.

In the second difference function, $G_{\mathrm{TiTi}}(r)$, shown in Fig. 3, a first peak at 2 Å is due to an incomplete subtraction of the Ti–O correlation. The three features at 3.5, 6 and 8 Å can be assigned to Ti–Ti atomic pairs. The first distance at 3.5 Å agrees with the Ti–Ti peak observed in a previous neutron diffraction study of a glass with the same composition (Wright et al., 1977; Yarker et al., 1986). However, our data have a higher *r*-space resolution due

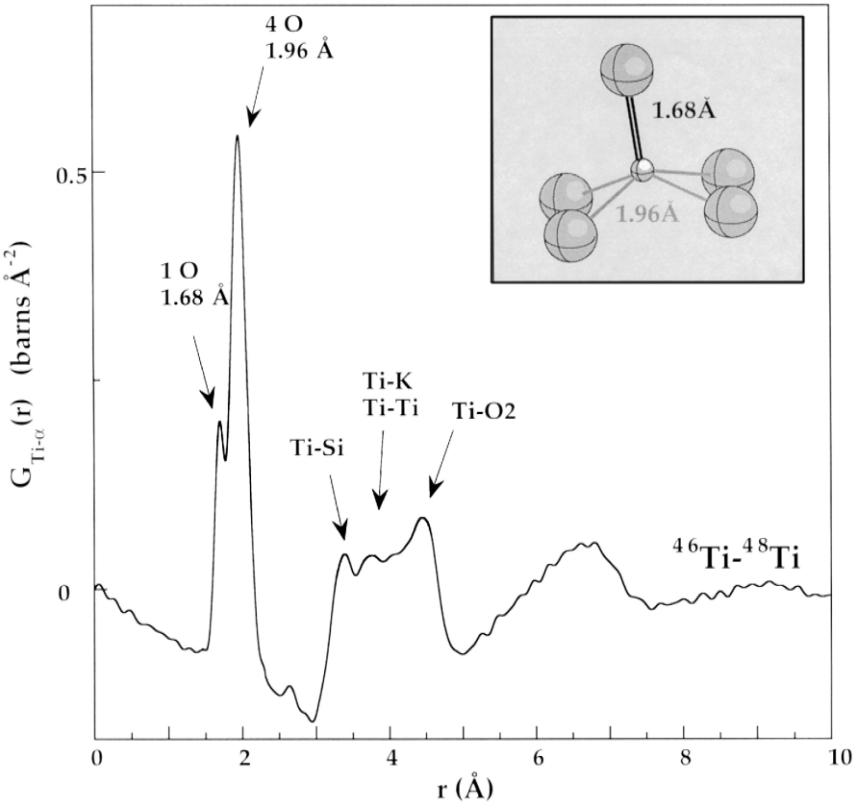

Fig. 2. First difference correlation function for Ti, $G_{\mathrm{Ti}-\alpha}(r)$. The inset shows the Ti site determined with isotopic substitution neutron diffraction data.

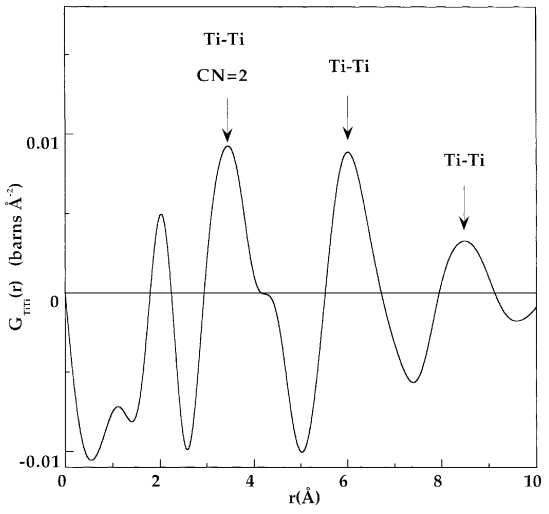

Fig. 3. Second difference correlation function for Ti, $G_{\mathrm{TiTi}}(r)$, obtained by Fourier transforming the signal $\Delta\,(\Delta_{\mathrm{Ti}-\alpha}(Q)) = {}^{48}\mathrm{S}(Q) - 2 * {}^{\mathrm{mix}}\mathrm{S}(Q)$. The peaks at 3.5, 6 and 8 Å correspond to Ti–Ti distances.

to a larger Q-space data range and an improved data statistics. The number of similarities between our $G_{\mathrm{TiTi}}(r)$ function and that of Wright et al., obtained from independent diffraction experiments on different specimens, is a good indication of the reproducibility of the second difference method. Due to the sizeable amount of errors in these second difference functions, it is impossible to obtain an exact determination of the coordination numbers and a discussion of the details of the peaks (as shoulders) is rather speculative.

A random distribution of Ti atoms predicts that each oxygen, excluding the oxygen involved in the titanyl bond, is linked to Ti and Si in the stoichiometric proportions of the glass composition. This gives a Ti–Ti coordination number of 1.3 in $K_2O \cdot TiO_2 \cdot 2SiO_2$ glass. A Gaussian fit of the peak at 3.5 Å indicates that about 2.0 Ti atoms lie around a central Ti atom, which was recently confirmed in a Ti K-edge EXAFS study (Farges, 1999). This experimentally determined value indicates that Ti is not randomly dispersed in the glass. The Ti–Ti distance at 3.5 Å corresponds to corner-sharing TiO_5 pyramids linked by their basal oxygen. This arrangement differs from that encountered in crystalline compounds. In titanates, TiO_5 pyramids are edge-sharing while in titanosilicates, there is no direct TiO_5–TiO_5 linkage and TiO_5 units are separated by one or two SiO_4 tetrahedra. The mineral fresnoite, $Ba_2TiSi_2O_8$, presents a composition close to that of the investigated glass, and is characterized by the presence of $Si_2O_7^{2-}$ groups (Moore and Louisnathan, 1969). In this mineral, TiO_5 sites are connected to the $Si_2O_7^{2-}$ groups. In addition to the oxygen atoms involved in the titanyl bond, oxygen atoms belong to Ti–O–Si and Si–O–Si linkages, excluding Ti–O–Ti linkages. This chemical ordering of oxygen atoms gives long Ti–Ti distances (6.07 Å). Natisite, Na_2TiSiO_5, only presents Ti–O–Si linkages (Nyman and O'Keefe, 1978), but the Ti–Ti distance of 4.6 Å is larger than that in the studied glass, despite a higher Ti concentration. In the two cases, the first cation coordination shell around Ti excludes Ti atoms, on the contrary to what we observe in the glass structure. This strong difference in the local topology between the glass and the crystalline phases of similar composition may explain the low tendency to devitrify for this glass (Bouhifd, 1995; Bouhifd et al., 1999).

A reverse Monte Carlo (RMC) modeling of this glass (Cormier et al., 1997) has shown that, on average, a TiO_5 polyhedron is linked to two other TiO_5 and two SiO_4 polyhedra and hence contributes to the polymerization of the network. Moreover, the simulated Ti–Si distance at 3.26 Å is consistent with corner-sharing SiO_4 and TiO_5 polyhedra. A representation of the Ti atoms in the RMC model is shown in Fig. 4, in which Ti–Ti atoms closer than 4.0 Å are shown as linked by a bond. The distribution of Ti atoms is clearly inhomogeneous with regions of high density of Ti atoms directly connected. This simulation cannot give a good estimate of the Ti domains because of the limited size of the model (the length of the cubic cell is 26.36 Å). However, the presence in the experimental $G_{\mathrm{TiTi}}(r)$ of a Ti–Ti correlation at 8 Å results from low radial disorder, which implies either a very well-ordered glass structure or Ti domains with a minimum diameter of 16 Å (Farges, 1999).

3.3. Cationic sites in glasses

Important analogies exist in the first difference functions obtained for various cations in silicate and aluminosilicate glasses (Fig. 5). This suggests that

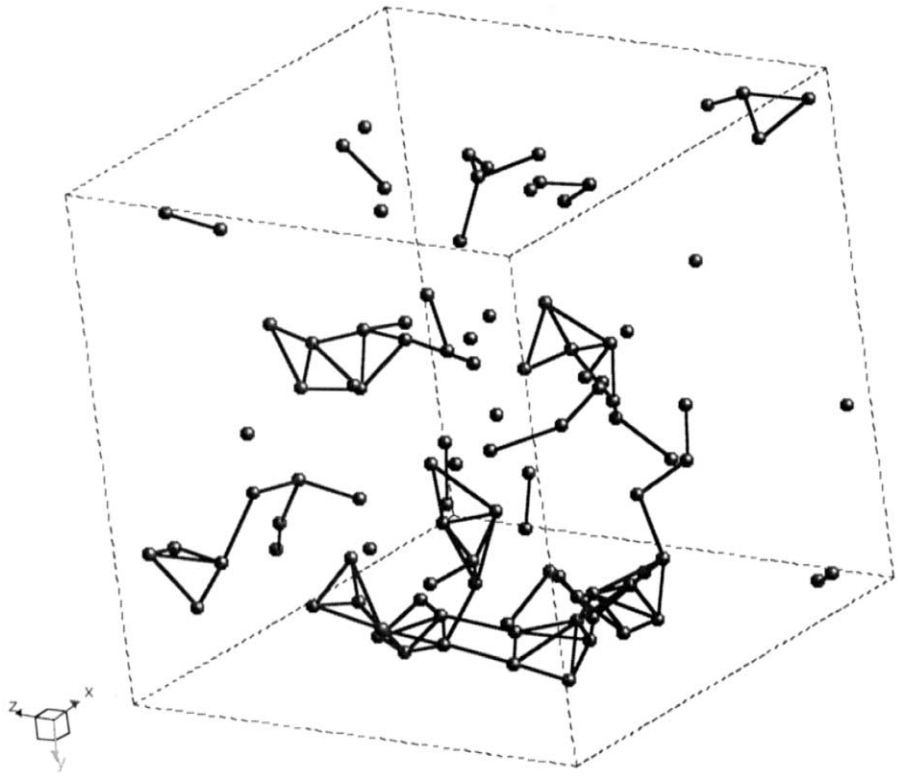

Fig. 4. Distribution of Ti atoms in the RMC model of the $K_2O \cdot TiO_2 \cdot 2SiO_2$ glass. Bonds indicate Ti nearest neighbor to another Ti. The cubic cell length is 26.36 Å.

cationic environments in glasses have similar characteristics. This local structural organization is independent of variations in cation concentration, e.g., 5.9 at.% for Ni in $Ca_2NiSi_3O_9$ vs. 14.3 at.% for Li in $LiAlSiO_4$, and in glass composition, encompassing silicate and aluminosilicate glasses. This is emphasized for Li where the $G_{Li-\alpha}(r)$ functions are similar in an aluminosilicate glass, $LiAlSiO_4$ (Fig. 5, top curve), where Li atoms are charge compensators and in a silicate glass, $Li_2Si_2O_5$, where Li atoms are modifiers (Zhao et al., 1998). Structural oscillations are discernible up to 10 Å in the $G_{M-\alpha}(r)$ functions, which indicates a well-defined cationic arrangement at medium-range distances.

All the $G_{M-\alpha}(r)$ functions have a first sharp intense peak which is due to the first shell of neighbors, indicating the presence of well-defined cationic sites (Table 1). These sites present cation–oxygen distances and cation coordination numbers which may be close to those observed in crystals of equivalent compositions (e.g., Li and Ti), for cations with low coordination numbers, in which a small radial disorder is expected. However, cations with larger coordination numbers present lower coordination numbers in the glass than in crystalline references of similar stoichiometry. This is the case of Ca (eight- and sixfold coordinated in crystalline $CaNiSi_2O_6$ and vitreous $Ca_2NiSi_3O_9$, respectively) and Ni (six- and fivefold coordinated in crystalline $CaNiSi_2O_6$ and vitreous $Ca_2NiSi_3O_9$, respectively). The cation–oxygen distances determined by neutron diffraction are similar to the distances derived from EXAFS, such as for Ca in $CaMgSi_2O_6$ glass (Combes et al., 1991), Ti in $K_2TiSi_2O_7$ glass (Farges et al., 1996) and Ni in $CaNiSi_2O_6$ glass (Galoisy and Calas, 1993a,b). These elements do not suffer strong inharmonic effects which would result in short apparent cation–oxygen distances in these glasses (Brown et al., 1995). Several cations are distributed among sites having fivefold coordination, such as Ti and Ni,

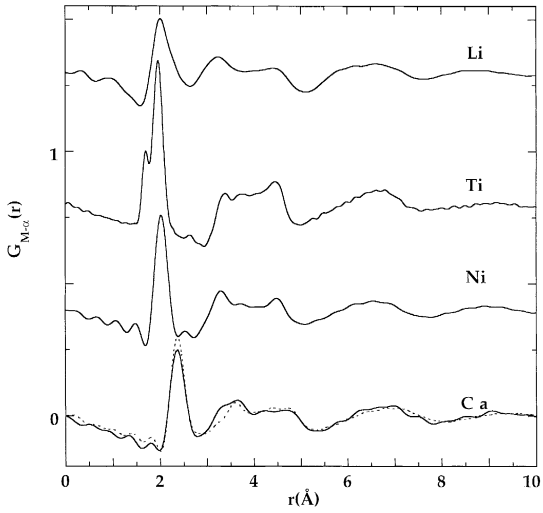

Fig. 5. Comparison of the first difference correlation functions, $G_{M-\alpha}(r)$, for Li in $Li_2O \cdot Al_2O_3 \cdot 2SiO_2$, Ti in $K_2O \cdot TiO_2 \cdot 2SiO_2$, Ni and Ca in $2CaO \cdot NiO \cdot 3SiO_2$, from top to bottom. The lower dashed curve in the $G_{Ca-\alpha}(r)$ function for Ca in $CaO \cdot SiO_2$ (Eckersley et al., 1988).

as well as divalent Fe, according to recent FeK-edge EXAFS studies (Brown et al., 1995).

Radial disorder effects may be quantified by neutron diffraction with isotopic substitution. The main cation–oxygen correlation shows standard deviation values, σ_{M-O}, which are similar for all glasses, about 0.1 Å. This indicates well-defined coordination shells. The extent of the data obtained by neutron diffraction in the *Q*-space gives then the possibility to resolve the various subshells which contribute to the definition of the site geometry. The good contrast for titanium isotopes allows the deconvolution of two Ti–O distances separated by 0.3 Å, indicating a square pyramid, with one short and four long bonds. This site distortion is due to the linkage of the TiO_5 pyramid to the glassy silicate network, and to the peculiar role of alkalis in this glass, K atoms being charge compensators of the non-bridging titanyl oxygen. Site distortions can be also precisely evaluated in the case of lithium-containing glasses (Uhlig et al., 1996; Cormier et al., 1998b; Zhao et al., 1998), considering the asymmetry of the first peak at high *r*-values. The good signal-to-noise ratio of the first difference functions, due to the high contrast between the scattering length of Li isotopes, explains that disorder may be resolved in terms of discrete Li–O contributions. Li atoms occur in tetrahedral sites in silicate, aluminosilicate and borate glasses, as in most crystalline silicates. However, the mean Li–O distance in silicate glasses or crystals is $d_{Li-O} \approx 1.96$ Å, i.e., shorter than in the aluminosilicate glass (2.1 Å); this behavior is due to the charge compensating role of Li in the latter as opposed to a network modifier role in the former. The presence of Li-distorted sites in the $LiAlSiO_4$ glass ($\Delta r = 0.3$ Å) is in relation with the presence of Al second neighbors (see below). An asymmetric distribution exists also for Ca and Ni in silicate glasses: in the two cases, the $G_{M-\alpha}(r)$ function shows a broad tail at high *r*-values, though an exact evaluation of these contributions is more difficult. Together with the

Table 1
Cationic sites in silicate glasses (interatomic distance, *R*, coordination number, *N*, standard deviation, σ) as derived from Gaussian fit of the neutron diffraction data

Atomic pairs	*R* (Å)	*N*	σ (Å)	Glass	Reference
Li–O1	1.97 ± 0.01	3.2 ± 0.1	0.12 ± 0.01	$Li_2Si_2O_5$	Zhao et al. (1998)
Li–O2	2.2 ± 0.05	0.8 ± 02	0.16 ± 0.02		
Li–O1	2.02 ± 0.01	2.8 ± 0.1	0.11 ± 0.01	$LiAlSiO_4$	Cormier et al. (1998b)
Li–O2	2.32 ± 0.02	1.1 ± 0.1	0.10 ± 0.02		
Ca–O1	2.37 ± 0.01	6.15 ± 0.17	0.12 ± 0.01	$CaSiO_3$	Gaskell et al. (1991)
Ca–O2	2.5–2.85	0.95 ± 0.2			
Ti–O1	1.68 ± 0.01	0.85 ± 0.1	0.05 ± 0.01	$K_2TiSi_2O_7$	Cormier et al. (1998a)
Ti–O2	1.96 ± 0.01	4 ± 0.1	0.1 ± 0.01		
Ni–O1	2.02 ± 0.01	4.8 ± 0.2	0.11 ± 0.01	$Ca_2NiSi_3O_9$	Gaskell et al. (1992)
Ni–O2	2.3–2.7	1.2 ± 0.2	0.3 ± 0.02		

presence of coordination numbers, which are lower in the glass than in crystals of similar compositions, these peculiar aspects of the cation–oxygen radial distribution functions can be considered as a property of the melt dynamics: fast rearrangements of configurations at high temperatures are an obstacle to high atomic correlation around a given cation. Such observations have been evidenced for Si MAS-NMR at high temperature and were used to explain rheologic properties of silicate melts (Farnan and Stebbins, 1994).

There is no indication from neutron diffraction whether the long bonds, which are evidenced in the broad tail at high *r*-values, correspond to specific sites of larger size than those corresponding to the main sharp peak or to specific bonds within an average site. An additional constraint on the structural models may be provided by the bond valence approach which describes the bond length–bond strength relationships for a given cation (Brese and O'Keefe, 1991). This method has been useful to infer structural models from the experimental interatomic distances (Galoisy and Calas, 1993a,b; Farges et al., 1994, 1996).

According to relation (2) in Brese and O'Keefe (1991), a site with only long bonds would correspond to strongly underbonded, unstable sites. This indicates that cations occur in average sites, in which normal and long bonds coexist. As these long bonds have a smaller bond strength than normal bonds do, they may correspond to bridging oxygens in order to satisfy the valence sum rule. Relation (2) in Brese and O'Keefe (1991) has been used for describing site stability in crystals and glasses. However, disorder effects in glasses lead to distribution in distances, which gives a modified expression of the bond valence of an element *i* surrounded by an atom *j* (Zhao et al., 1998):

$$\nu_{ij} = \exp\left(\frac{R_0 - R_{\exp}}{B}\right)\exp\left(\frac{\sigma^2}{2B^2}\right), \qquad (11)$$

where $R_0 = 1.466$ Å and $B = 0.37$ Å are atom-dependent parameters (Brese and O'Keefe, 1991) and σ is the standard deviation of the distribution. By including the contribution at high *r*-values, the bond valence sum ($\Sigma\nu_{ij} = 0.98$) is closer from the expected valence of 1 for Li^+ in $Li_2O \cdot 2SiO_2$ glass than without the contribution at long distance ($\Sigma\nu_{ij} = 0.86$).

3.4. Beyond the coordination shell

Between 3 and 5 Å, all the $G_{M-\alpha}(r)$ functions exhibit a split second peak related to second neighbors. These peaks appear for distances close to those of compositionally equivalent crystals, which indicates that some structural crystalline arrangements are maintained in the glass structure. A comparison of the experimental $G_{Ca-\alpha}(r)$ function for vitreous $CaSiO_3$ with the one calculated for crystalline $CaSiO_3$ shows a qualitative agreement between the experimental and simulated curves (Eckersley et al., 1988). The peak at 3.5 Å corresponds to the Ca–Ca and Ca–Si distances in $CaSiO_3$ crystal and the component near 4.4 Å is at the same distance as the Ca–O(2) pair in crystalline $CaSiO_3$. However, the simulation on $CaSiO_3$ shows the presence of additional peaks in the crystal beyond 5 Å, which contradicts the possibility of microcrystallites models. Contrary to crystals, a structural deficit exists around 5–6 Å for all studied cations in glasses The differential correlation function for Sr in silicate glasses obtained by AWAXS shows also a lack of correlations for this range (Creux et al., 1995).

Compared to the previously studied Ca-metasilicate glass (Eckersley et al., 1988; Gaskell et al., 1991), a third of the Ca atoms has been replaced by Ni atoms in the $Ca_2NiSi_3O_9$ glass. The comparison of the neutron diffraction data for these two compounds can thus give insights on the structural cationic modifications when a cation is substituted by another. The determination of how the cationic environment of a cation is affected by the presence of another cation is an important question to explain the mixed alkali effect (Maass, 1999). The $G_{Ca-\alpha}(r)$ function obtained for the mixed Ca–Ni silicate glass can be compared with that obtained on the $CaSiO_3$ glass (Eckersley et al., 1988). The two functions are very similar overall the *r*-range except for a shoulder present in the $Ca_2NiSi_3O_9$ glass at 3.3 Å and absent in the $CaSiO_3$ glass. This distance is close to that observed in Ni-diopside crystal at 3.2 Å (Cameron et al., 1973), corresponding to a Ca–Ni contribution. A distinct peak at 3.3 Å is also observed in the

$G_{Ni-\alpha}(r)$ function (Fig. 5). Therefore, this feature in the glass spectra is likely due to a Ca–Ni correlation. The similitude between the two function indicates that the local- and medium-range environment around Ca is little affected by the replacement of Ca by Ni.

Li provides an interesting comparison between silicate and aluminosilicate glasses. In aluminosilicate crystals, each LiO_4 tetrahedron shares two edges with $(Si,Al)O_4$ tetrahedra, yielding to unusually short Li–(Si,Al) distances ($\sim$2.6–2.7 Å). The strong repulsion between Li and (Si,Al) cations is balanced by short O–O shared edges and long Li–O distances. The same mean Li–O distance in $LiAlSiO_4$ glass and crystal suggests the formation of edge-linked tetrahedra in the glass. A regular site for Li with smaller Li–O distances will induce some distortion of the aluminosilicate network which is not energetically favored. By contrast, in silicate glasses, the Li–O distance of 1.96 Å indicates corner-sharing tetrahedra as in related crystals, which is supported by higher Li–Si distances ($\sim$3.2 Å) (Zhao et al., 1998). These results indicate significant differences in the local geometry of Li depending on whether Li is a charge compensator in an interstitial site (in aluminosilicates) or a network modifier (in silicates).

Above 5 Å, broad contributions centered near 7 and 9 Å are observed and do not correspond to those observed in crystals. The distance of 5 Å can thus be considered as a size limit of the structural organizations that are similar in silicate glasses and crystals. At greater distances, partial pair distribution functions observed for the periodic compounds are lost in the glasses. However, evidence for important order above 5 Å can still be observed in selecting cation–cation atomic pairs, either experimentally with the second difference function or numerically by molecular dynamics calculations (Abramo et al., 1992).

3.5. Cation ordering in glasses

The correlation functions obtained in silicate glasses by double difference for Ti (Cormier et al., 1998a), Ni (Gaskell et al., 1992), Ca (Gaskell et al., 1991) and Li (Zhao et al., 1998) reveal similar structural features (Fig. 6). Homogeneous cation–cation distances, R_{MM}, can be calculated considering densely packed spheres centered on an M atom and

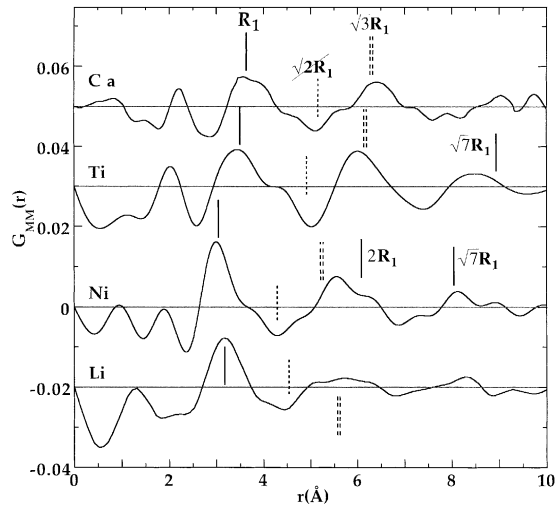

Fig. 6. Comparison of the second difference correlation function, $G_{MM}(r)$, for Ca in $CaO \cdot SiO_2$ (Gaskell et al., 1991) Ti in $K_2O \cdot TiO_2 \cdot 2SiO_2$, Ni in $2CaO \cdot NiO \cdot 3SiO_2$ and Li in $LiSi_2O_5$ (Zhao et al., 1998), from top to bottom. R_1 is the first $M-M$ distance and other $M-M$ contributions appear near $\sqrt{3}R_1$, $2R_1$ and $\sqrt{7}R_1$ but no contributions are visible near $\sqrt{2}\ R_1$.

taking the random packing fraction of 0.63. The volume of a sphere is related to the volume, V_M, occupied by each M atom with the relation:

$$\frac{4}{3}\pi R^3 = 0.63 V_M,$$

where $2R = R_{MM}$ and $V_M = (c_M \rho_0)^{-1}$, with c_M the atomic fraction of M atoms and ρ_0 the atomic number density. The average cation–cation distance predicted by a homogeneous distribution is:

$$R_{MM} = (6 \times 0.63 / \pi \rho_0 c_M)^{1/3}. \quad (12)$$

According to relation (12), a homogeneous distribution of Ti atoms corresponds to a typical first cation–cation distance close to 6 Å. An important first cation–cation contribution at short distances is present in all spectra and is then a clear indication of non-homogeneous distribution of cations in glasses.

This inhomogeneous distribution of cations, the presence of a peak near 8 Å in $G_{MM}(r)$ (Fig. 6), and the fact that the longer cation–cation distances are related to the nearest cation–cation distance support the concept of medium-range organization of cations in the glass structure, within domains extending over

at least 9–10 Å (Table 2). Specifically, if R_1 is the first M–M distance, the second lies near $\sqrt{3}R_1$ and the third near $\sqrt{7}R_1$. Moreover, a distance at $\sqrt{2}R_1$, which is characteristic of an out-of-plane polyhedra linkage, is lacking. As previously proposed for Ca and Ni silicate glasses (Gaskell, 1991; Gaskell et al., 1991), these specific cation–cation distances can be associated with a two-dimensional ordering of cations at medium range. However, edge-sharing polyhedra are generally observed in densely packed domains of low-charge cations such as Ca and Ni, as corner-shared polyhedra occur in the Ti-containing glass. This important structural property of Ti in a silicate glass has not been demonstrated before, owing to the local character of spectroscopic methods such as EXAFS. The bidimensional character of the Ti-rich regions and the proximity of K near Ti for the charge compensation of the titanyl oxygen explain the high thermal stability of the $K_2O \cdot TiO_2 \cdot 2SiO_2$ glass, in contrast to the nucleating role of this element in other glass compositions (Dumas and Petiau, 1986; Dumas et al., 1985).

Similar cation–cation distances are evidenced by X-ray diffraction on silicate or borate glasses containing heavy elements, the distribution of which dominates the experimental structure factor. These studies reveal cation–cation correlations near 4, 7 and 10 Å in silicate (Brosset, 1963; Hanson and Egami, 1986) and borate (Krogh-Moe, 1962; Block and Piermarini, 1964; Yasui et al., 1988, 1990) glasses, over a wide range of composition (3–65 mol% of non-network forming oxides). A recent AWAXS study of the SrK-edge on a silicate glass has also shown Sr–Sr distances at 4 and 7 Å (Creux et al., 1995). This heterogeneous structure of glasses is also supported by numerical modeling (Abramo et al., 1992; Cormier et al., 1997, 1999), which is able to reproduce cationic-rich regions consistent with the crystalline structures (Abramo et al., 1992).

The structural information brought by neutron diffraction with isotopic substitution suggests that cations occur in well-defined sites which, in silicate glasses, are ordered in domains, the radius of which extends up to 10 Å. As the polymeric network and the cationic domains are linked through non-bridging oxygens, cation ordering is expected to exert an influence on glass properties. It has been suggested that crystalline nucleation, ionic conduction or thermodynamic properties may be influenced by cationic structural organization at medium-range scale (Cormier et al., 1998a,b). For instance, the inhomogeneous distribution of cations in glasses is dependent on the role these cations play in the glass structure. Li–Li distances are different in silicate and aluminosilicate glasses, 3.1 and 5 Å, respectively. In the former, these short distances correspond to edge-sharing LiO_4 tetrahedra, as in the latter Li occurs in the vicinity of AlO_4 tetrahedra with Al–Al distances of about 5 Å. This strong difference in cationic ordering has been used to explain the decrease in the activation energy for Li diffusion in glasses as SiO_2 is replaced by Al_2O_3 (Cormier et al., 1998b).

Recent studies on the supercooled liquids suggest the presence of structural hetereogeneities ("frustration-limited domains": Kivelson et al., 1994, 1995; "structured cluster aggregation": Oguni, 1997). These domains, whose size and degree of ordering increase as T decreases, can form dynamic heterogeneities of roughly 30 Å (Ediger et al., 1996), which are responsible for the slow structural relaxations as T_g is approached from above. Strong support for spatial

Table 2
Cation–cation distances and number of cationic neighbors derived from neutron diffraction data in silicate glasses

Atomic pairs	R (Å)	N	Glass	Reference
Li–Li	3.1 ± 0.05	4 ± 1	$Li_2Si_2O_5$	Zhao et al. (1998)
Li–Li	5		$LiAlSiO_4$	Cormier et al. (1998b)
Ca–Ca1	3.7	5.2	$CaSiO_3$	Gaskell et al. (1991)
Ca–Ca2	4.5	0.95 ± 0.2		
Ca–Ca	3.7	5	$Ca_2NiSi_3O_9$	Gaskell et al. (1992)
Ti–Ti	3.5	2	$K_2TiSi_2O_7$	Cormier et al. (1998a)
Ni–Ni	3.03	1	$Ca_2NiSi_3O_9$	Gaskell et al. (1992)

heterogeneities in dynamics has been derived in recent computer simulations (Donati et al., 1998; Hiwatari and Muranaka, 1998; Wilson and Madden, 1998). The concept of non-homogeneous glass structure (Greaves, 1989) is, hence, in agreement with these density fluctuations in the supercooled liquids. Furthermore, intermediate range order has been proposed to explain the "boson" peak of light and neutron inelastic scattering (Quitmann and Soltwisch, 1998). The explanation suggests that the 'boson' peak and the vibrational density of states "excess" are a result of vibrations localized in more cohesive domains of size $l \approx 20$ Å (Duval et al., 1990; Pocsik and Koos, 1990). The cation-rich regions evidenced by neutron diffraction with isotopic substitution are of the same order of size (≈ 15–20 Å) and could be related to the various nano-inhomogeneities proposed in the models of structural relaxation or plastic deformation and used to interpret the excess in the low-energy vibrational density of states.

4. Conclusions

Neutron diffraction with isotopic substitution is a powerful technique to investigate the structure of glasses. In addition to defining the cationic coordination shell, it gives an accurate description of the radial disorder of cation–oxygen bonds owing to the large range of Q-space accessible. First difference functions obtained for Ti, Li, Ca and Ni in silicate glasses show strong similarities in their medium-range structure. The most original information concerns cation distribution inside the glass structure, which can be isolated by the double difference method. First cation–cation distances, R_1, always indicate an important contribution of edge- or corner-sharing cationic polyhedra in silicate glasses. By contrast, the $LiAlSiO_4$ glass exhibits a random distribution of Li, in relation with the charge-compensating role of Li cations. The observation, in silicate glasses, of second and third cation–cation distances, at $\sqrt{3}R_1$ and $\sqrt{7}R_1$, indicates the presence of cation-rich regions which can be described as two-dimensional cationic arrangements extending up to 10 Å in diameter. These domains appear to be a key property of silicate glasses, which help in rationalizing glass physical and chemical properties.

Acknowledgements

We would like to thank the two anonymous reviewers for their helpful comments. The content of this paper has benefited from discussions during the Arc et Sénans Workshop on Silicate Melts, and we wish to thank the organizers, Don Dingwell and Pascal Richet. This is IPGP contribution no. 1648.

References

Abramo, M.C., Caccamo, C., Pizzimenti, G., 1992. Structural properties and medium-range order in calcium-metasilicate ($CaSiO_3$) glass: a molecular dynamics study. J. Chem. Phys. 96, 9083–9091.

Block, S., Piermarini, G.J., 1964. Alkaline Earth cation distributions in vitreous borates. Phys. Chem. Glasses 5, 138–143.

Bouhifd, M.-A., 1995. Propriétés thermodynamiques de minéraux et liquides d'intérêt géophysique. PhD Thesis, Université Paris 7, Denis Diderot.

Bouhifd, M.A., Sipp, A., Richet, P., 1999. Heat capacity, viscosity, and configurational entropy of alkali titanosilicate melts. Geochim. Cosmochim. Acta 63, 2429–2437.

Brese, N.E., O'Keefe, M., 1991. Bond valence parameters in solids. Acta Crystallogr., Sect. B 47, 192–197.

Brosset, C., 1963. X-ray investigation of the distribution of heavy atoms in glass. Phys. Chem. Glasses 4, 99–102.

Brown Jr., G.E., Farges, F., Calas, G., 1995. X-ray scattering and X-ray spectroscopy studies of silicate melts. In: Stebbins, J.A., Dingwell, D., McMillan, P. (Eds.), Structure, Dynamics, and Properties of Silicate Melts. Rev. Mineral. 32, pp. 317–410.

Cameron, M., Sueno, S., Prewitt, C.T., Papike, J.J., 1973. High-temperature crystal chemistry of acmite, diopside, hedenbergite, jadeite, spodumene and ureyite. Am. Mineral. 58, 594–618.

Combes, J.M., Brown Jr., G.E., Waychunas, G.A., 1991. X-ray absorption study of the local Ca environment in silicate glasses. In: Hasnain, S.S. (Ed.), XAFS VI. Ellis Horwood, Chichester, pp. 312–314.

Cormier, L. 1996. Étude structurale de l'environnement de cations dans des verres d'oxydes par diffraction des neutrons. PhD Thesis, Université Paris 6, Paris.

Cormier, L., Creux, S., Galoisy, L., Calas, G., Gaskell, P.H., 1996. Medium-range order around cations in silicate glasses. Chem. Geol. 128, 77–91.

Cormier, L., Calas, G., Gaskell, P.H., 1997. A reverse Monte Carlo study of a titanosilicate glass. J. Phys.: Condens. Mater. 9, 10129–10136.

Cormier, L., Gaskell, P.H., Calas, G., Soper, A.K., 1998a. Medium-range order around titanium in a silicate glass studied by neutron diffraction with isotopic substitution. Phys. Rev. [Sect.] B 58, 11322–11330.

Cormier, L., Gaskell, P.H., Calas, G., Zhao, J., Soper, A.K., 1998b. Environment around Li in the $LiAlSiO_4$ ionic conduc-

tor glass: a neutron scattering and reverse Monte Carlo study. Phys. Rev. [Sect.] B 57, R8067–R8070.

Cormier, L., Calas, G., Creux, S., Gaskell, P.H., Bouchet-Fabre, B., Hannon, A.C., 1999. Environment around strontium in silicate and aluminosilicate glasses. Phys. Rev. [Sect.] B 59, 13517–13520.

Creux, S., Bouchet-Fabre, B., Gaskell, P.H., 1995. Anomalous wide angle X-ray scattering study of strontium silicate and aluminosilicate glasses. J. Non-Cryst. Solids 192/193, 360–363.

Donati, C., Douglas, J.F., Kob, W., Plimpton, S.J., Poole, P.H., Glotzer, S.C., 1998. String-like cooperative motion in a supercooled liquid. Phys. Rev. Lett. 80, 2338–2341.

Dumas, T., Ramos, A., Gandais, M., Petiau, J., 1985. Role of zirconium in nucleation and crystallization of a (SiO_2 Al_2O_3, MgO, ZnO) glass. Mater. Sci. Lett. 4, 129–132.

Dumas, T., Petiau, J., 1986. EXAFS study of titanium and zinc environments during nucleation in a cordierite glass. J. Non-Cryst. Solids 81, 201–220.

Duval, E., Boukenter, A., Achibat, T., 1990. Vibrational dynamics and the structure of glasses. J. Phys.: Condens. Matter 2, 10227–10234.

Eckersley, M.C., Gaskell, P.H., Barnes, A.C., Chieux, P., 1988. The environment of Ca ions in silicate glasses. J. Non-Cryst. Solids 106, 132–136.

Ediger, M.D., Angell, C.A., Nagel, S.R., 1996. Supercooled liquids and glasses. J. Phys. Chem. 100, 13200–13212.

Faber, T.E., Ziman, J.M., 1964. A theory of the electrical properties of liquid metals: III. The resistivity of binary alloys. Philos. Mag. 11, 153–173.

Farges, F., 1999. A TiK-edge EXAFS study of the medium range environment around Ti in oxide glasses. J. Non-Cryst. Solids 244, 25–33.

Farges, F., Brown Jr., G.E., Calas, G., Galoisy, L., Waychunas, G.A., 1994. Structural transformation in Ni-bearing $Na_2Si_2O_5$ glass and melt. Geophys. Res. Lett. 21, 1931–1934.

Farges, F., Brown Jr., G.E., Navrotsky, A., Gan, H., Rehr, J.J., 1996. Coordination chemistry of Ti(IV) in silicate glasses and melts: II. Glasses at ambient temperature and pressure. Geochim. Cosmochim. Acta 60, 3039–3053.

Farnan, I., Stebbins, J.F., 1994. The nature of the glass transition in a silica-rich oxide melt. Science 265, 1206–1208.

Galoisy, L., Calas, G., 1993a. Structural environment of nickel in silicate glass/melt systems: I. Spectroscopic determination of coordination states. Geochim. Cosmochim. Acta 57, 3613–3626.

Galoisy, L., Calas, G., 1993b. Structural environment of nickel in silicate glass/melt systems: II. Geochemical implications. Geochim. Cosmochim. Acta 57, 3627–3633.

Gaskell, P.H., 1991. Models for the structure of amorphous solids. In: Cahn, R.W., Haasen, P., Kraner, E.J. (Eds.), Materials Science and Technology 9. VCH, Weinheim, pp. 175–278.

Gaskell, P.H., 1993. Neutron contrast techniques applied to oxide glasses. In: Suck, J.B., Chieux, P., Raoux, D., Rielke, C. (Eds.), Methods in Determination of Partials Structure Factors of Disordered Matter by Neutron and Anomalous X-ray Diffraction. World Scientific Publ., Singapore, pp. 34–45.

Gaskell, P.H., Eckersley, M.C., Barnes, A.C., Chieux, P., 1991. Medium-range order in the cation distribution of a calcium silicate glass. Nature 350, 675–677.

Gaskell, P.H., Zhao;, Z., Calas, G., Galoisy, L., 1992. The structure of mixed cation oxide glasses. In: Pye, L.D., La-Course, W.C., Stevens, H.J. (Eds.), The Physics of Non-Crystalline Solids. Taylor and Francis, London, pp. 53–58.

Greaves, G.N., 1989. EXAFS, glass structure and diffusion. Philos. Mag. B 60, 793–800.

Hannon, A.C., Howells, W.S., Soper, A.K., 1990. ATLAS: a suite of programs for the analysis of time-of-flight neutron diffraction data from liquid and amorphous samples. In: Johnson, M.W. (Ed.), IOP Conf. Ser. Neutron Scattering Data Analysis 107, 193.

Hanson, C.D., Egami, T., 1986. Distribution of Cs^+ ions in single and mixed alkali silicate glasses from energy dispersive X-ray diffraction. J. Non-Cryst. Solids 87, 171–184.

Hiwatari, Y., Muranaka, T., 1998. Structural heterogeneity in supercooled liquids and glasses. J. Non-Cryst. Solids 235–237, 19–26.

Kivelson, S.A., Zhao, X., Kivelson, D., Fischer, T.M., Knobler, C.M., 1994. Frustration-limited clusters in liquids. J. Chem. Phys. 101, 2391–2397.

Kivelson, D., Kivelson, S.A., Zhao, X., Nussinov, Z., Tarjus, G., 1995. A thermodynamic theory of supercooled liquids. Physica A 219, 27–38.

Krogh-Moe, J., 1962. An X-ray study of barium borate glasses. Phys. Chem. Glasses 3, 208–212.

Maass, P., 1999. Towards a theory for the mixed alkali effect in glasses. J. Non-Cryst. Solids 255, 35–46.

Moore, P.B., Louisnathan, S.J., 1969. The crystal structure of fresnoite $Ba_2(TiO)Si_2O_7$. Z. Kristallogr. 130, 438–448.

Nyman, H., O'Keefe, M., 1978. Sodium titanium silicate, Na_2TiSiO_5. Acta Crystallogr., Sect. B 34, 905–906.

Oguni, M., 1997. 'Intracluster rearrangement' model for the α-process in supercooled liquids, as opposed to 'cooperative rearrangement of whole molecules within a cluster'. J. Non-Cryst. Solids 210, 171–177.

Poulsen, H.F., Neuefeind, J., Neumann, H.-B., Schneider, J.R., Zeilder, M.D., 1995. Amorphous silica studied by high-energy X-ray diffraction. J. Non-Cryst. Solids 188, 63–74.

Pocsik, I., Koos, M., 1990. Cluster size determination in amorphous structures using the boson peak. Solid State Commun. 74, 1253–1256.

Quitman, D., Soltwisch, M., 1998. Intermediate-range-order and the liquid ↔ glass transformation. Phil. Mag. B 77, 287–296.

Soper, A.K., Howell, W.S., Hannon, A.C., 1989. ATLAS — analysis time-of flight diffraction data from liquid and amorphous samples. Rutherford Appleton Laboratory Report, RAL-89-046.

Uhlig, H., Hoffmann, M.J., Lamparter, H.P., Aldinger, F., Bellissent, R., Steeb, S., 1996. Short-range order and medium-range order in lithium silicate glasses: I. Diffraction experiments and results. J. Am. Ceram. Soc. 79, 2833–2838.

Waseda, Y., 1984. Novel Applications of Anomalous (Resonance) X-ray Scattering for Structural Characterization of Disordered Materials. Springer-Verlag, Berlin.

Waseda, Y., Suito, H., 1977. The structure of molten alkali metal silicates. Trans. ISIJ 17, 82–91.

Wilson, M., Madden, P.A., 1998. Voids, layers, and the first sharp diffraction peak in $ZnCl_2$. Phys. Rev. Lett. 80, 532–535.

Wright, A.C., 1974. The structure of amorphous solids by X-ray and neutron diffraction. Adv. Struct. Res. Diffr. Methods 5, 1–84.

Wright, A.C., Yarker, C.A., Johnson, P.A.V., Wedgwood, F.A., 1977. Neutron scattering techniques for structural studies of amorphous solids. In: Frischat, G.H. (Ed.), Non-Crystalline Solids. TransTech. pp. 118–123.

Yarker, C.A., Johnson, P.A.V., Wright, A.C., Wong, J., Greegor, R.B., Lytle, F.W., Sinclair, R.N., 1986. Neutron diffraction and EXAFS evidence for TiO_5 units in vitreous $K_2O \cdot TiO_2 \cdot 2SiO_2$. J. Non-Cryst. Solids 79, 117–136.

Yasui, I., Hasegawa, H., Suito, Y., 1988. Structure of borate glasses containing Tl and Ba oxide. J. Non-Cryst. Solids 106, 30–33.

Yasui, I., Hasegawa, H., Saito, Y., Akasaka, Y., 1990. Structure of borate glasses containing heavy metal ions. J. Non-Cryst. Solids 123, 71–74.

Zhao, J., Gaskell, P.H., Cluckie, M.M., Soper, A.K., 1998. A neutron diffraction, isotopic substitution study of the structure of $Li_2O \cdot 2SiO_2$ glass. J. Non-Cryst. Solids 232–234, 721–727.

Zotov, N., Keppler, H., Hannon, A.C., Soper, A.K., 1996. The effect of water on the structure of silicate glasses — a neutron diffraction study. J. Non-Cryst. Solids 202, 153–163.